

Active Terahertz Nanoantennas Based on VO₂ Phase Transition

Minah Seo,^{†,‡} Jisoo Kyoung,^{†,‡} Hyeongryeol Park,[†] Sukmo Koo,[‡] Hyun-sun Kim,[†] Hannes Bernien,[†] Bong Jun Kim,[§] Jong Ho Choe,^{||} Yeong Hwan Ahn,[⊥] Hyun-Tak Kim,[§] Namkyoo Park,[‡] Q-Han Park,^{||} Kwangjun Ahn,^{*,†} and Dai-sik Kim^{*,†}

[†]Center for Subwavelength Optics and Department of Physics and Astronomy, Seoul National University, Seoul 151-747, Korea, [‡]Photonic Systems Laboratory, School of EECS, Seoul National University, Seoul 151-744, Korea, [§]Metal-Insulator Transition Lab., ETRI, Daejeon 305-350, Korea, ^{||}Department of Physics, Korea University, Seoul 136-701, Korea, and [⊥]Division of Energy Systems Research, Ajou University, Suwon 443-749, Korea

ABSTRACT Unusual performances of metamaterials such as negative index of refraction, memory effect, and cloaking originate from the resonance features of the *metallic composite atom*^{1–6}. Indeed, control of metamaterial properties by changing dielectric environments of thin films below the metallic resonators has been demonstrated^{7–11}. However, the dynamic control ranges are still limited to less than a factor of 10,^{7–11} with the applicable bandwidth defined by the sharp resonance features. Here, we present ultra-broad-band metamaterial thin film with colossal dynamic control range, fulfilling present day research demands. Hybridized with thin VO₂ (vanadium dioxide)^{12–18} films, nanoresonator supercell arrays designed for one decade of spectral width in terahertz frequency region show an unprecedented extinction ratio of over 10000 when the underlying thin film experiences a phase transition. Our nanoresonator approach realizes the full potential of the thin film technology for long wavelength applications.

KEYWORDS Terahertz spectroscopy, phase transition device, nanoantenna, terahertz active device, terahertz VO₂

Thin layers of semiconductors,¹⁹ superconductors,²⁰ correlated electron systems,²¹ and polymers²² are the core elements of modern science and technology. The dielectric properties of these thin films, actively changeable by optical,^{9,10,23,24} electrical,⁸ or thermal²⁰ means, with^{7,8} or without lateral patterns,²⁵ are used to control technologically important terahertz (THz) electromagnetic waves.^{26–34} For instance, a dynamic range of up to 10^{7,8} has been realized in metamaterial devices on semiconductor substrate whose dielectric properties are controlled by voltage. These attempts, however, are met with only partial success because thin films of $\lambda/100 \sim \lambda/100000$ thicknesses tend to be transparent to electromagnetic waves. In the limit of vanishingly small optical thickness, nearly constructive multiple interference³⁵ tends transmittance toward unity causing the thin film to be essentially invisible, making complete extinction nearly impossible even when the dielectric constants become very large. For example, the dramatic change in dielectric constant in VO₂ at 1 THz, from order of 1 to order of 10000, when used to control terahertz electromagnetic wave transmission, results in only a 20% change for a $\lambda/15000$ (20 nm) thick film.¹⁵

Clearly, we need a new scheme to boost the dynamic range of the control despite the limit posed by the huge disparity between terahertz wavelength and thickness of the film, to take full advantage of the opportunity offered by phase transition materials.^{13–17} Can we translate, say, the 4 orders of magnitudes change in dielectric constant associated with VO₂ phase transition, into the same 4 orders of magnitude change in extinction, thereby enabling the nano-scale thin film technology to fully enter into the long-wavelength applications? Our strategy is to add a nanostructure pattern, an array of nano slot antennas in a gold layer on top of the VO₂ thin film (Figure 1a). For the insulating VO₂, a rectangular hole in a gold coating acts as a slot antenna at resonance that receives nearby electromagnetic waves and funnels them into the other side of the slot.^{36–40} Therefore, the sample, when the VO₂ film is insulating, is essentially transparent to the incoming terahertz waves at resonance because the antenna is at an on state (Figure 1b). In stark contrast to the insulating state, when the film undergoes phase transition, the nano slot antenna no longer operates (off state), and therefore simple reflection occurs throughout the metallic part of the sample, leaving very small transmittance defined by the coverage.

We pattern rectangular hole arrays of length L and width w by electron beam lithography using a negative photoresist. The virgin sample prior to nanopatterning consists of a 100 nm thick VO₂ film deposited on a 430 μm thick sapphire substrate via reactive rf-magnetron sputtering.¹⁵ The rectangle arrays with widths of 27 μm , 1 μm , and 450 nm,

* To whom correspondence should be addressed. Kwangjun Ahn, phone, +82-2-880-4392; fax, +82-2-882-6595, e-mail, kwangjun@phya.snu.ac.kr. Daisik Kim, phone, +82-2-880-8174; fax, +82-2-882-6595; e-mail, dsk@phya.snu.ac.kr.

[‡] These authors contributed equally to this work.

Received for review: 01/20/2010

Published on Web: 05/14/2010



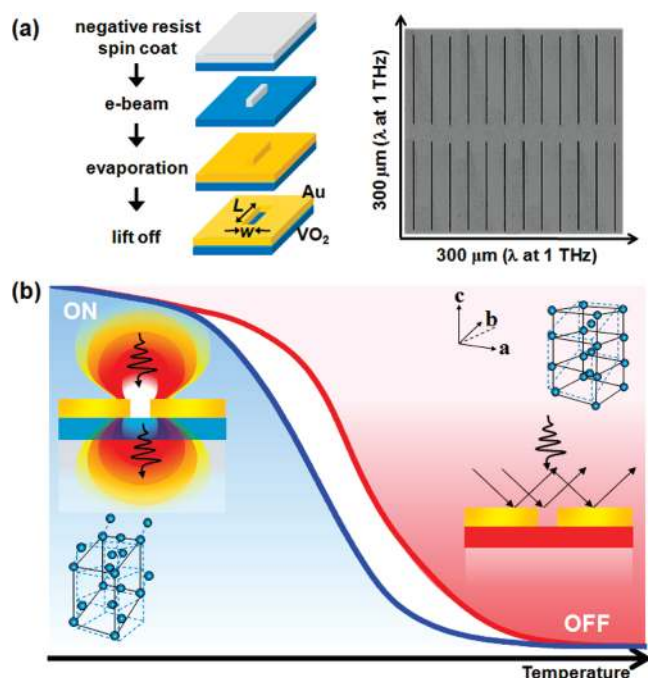


FIGURE 1. Schematic fabrication procedure of gold micro and nano slot antennas attached to VO₂ thin film and temperature-controlled terahertz resonant switching device. (a) The micro- and nanoantennas are fabricated by using negative type of photoresist patterning (left). Scanning electron microscopy (SEM) image of a nanoantenna pattern sample (30 μm period, 150 μm length, 450 nm width) (right). (b) Phase transition diagram of the nanopatterned VO₂ thin film as a function of temperature, seen through transmission. While the nanoantenna patterned on the insulating VO₂ thin film colored by blue is almost transparent to the resonant terahertz electromagnetic wave, in the metallic state colored by red it is completely opaque to the same incident wave due to drastically enhanced extinction.

respectively, and periods of 100, 100, and 30 μm, respectively, were fabricated on 100 nm thick gold deposited on VO₂/Al₂O₃ substrate, with fixed $L = 150 \mu\text{m}$. The rectangle array/VO₂ samples are mounted on a temperature-controlled stage. An ultra-broad-band slot antenna array, which we will discuss in later, is fabricated with the same method. The dimension of the antenna array is described in Figure 3.

The most straightforward method of examining our terahertz nano metamaterial performance is to measure transmission using the time domain terahertz spectroscopy.^{29,33,41–43} We used a single-cycle terahertz source generated from a 2 kV/cm biased semi-insulating GaAs emitter illuminated by a femtosecond Ti:sapphire laser pulse train of wavelength 780 nm, 76 MHz repetition rate, and 150 fs pulse width, to perform terahertz time-domain spectroscopy.³³ The p-polarized terahertz pulses with polarization perpendicular to the long axes of rectangles are incident on the sample. An electro-optic sampling method was used to detect the transmitted terahertz waves in time domain, in which an optical probe pulse undergoes a slight polarization rotation by the synchronized terahertz beam in a (110) oriented ZnTe crystal, detecting the horizontal electric field.

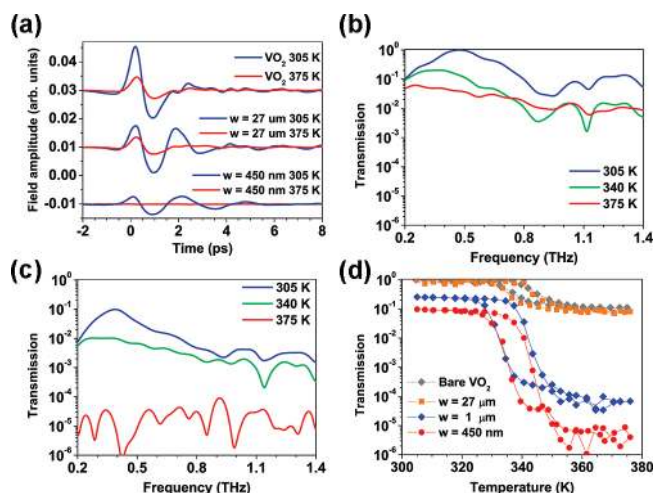


FIGURE 2. Temperature-dependent transmittance curves of terahertz metamaterials. (a) Time-domain transmitted field amplitude signals for the unpatterned (top), micropatterned (middle, $w = 27 \mu\text{m}$), and nanopatterned (bottom, $w = 450 \text{ nm}$) samples before (blue lines, 305 K) and after (red lines, 375 K) insulator-to-metal phase transition. The logarithmic plot for temperature-dependent transmittance spectra of the terahertz wave through the (b) 27 μm and (c) 450 nm width antenna array on the VO₂ film are shown. (d) Temperature-dependent hysteresis curves of a bare VO₂ thin film (gray diamonds), 27 μm (orange squares), 1 μm (blue diamonds), and 450 nm (red circles) width antenna array on the VO₂ film. The length is fixed to 150 μm (the resonance peak at 0.4 THz), and periods for row and column are 100 and 30 μm, respectively. Each hysteresis curve is measured at the resonance frequency 0.4 THz.

Figure 2a compares time-domain transmission signals of the unpatterned (top), micropatterned (middle, width $w = 27 \mu\text{m}$), and nanopatterned (bottom; $w = 450 \text{ nm}$) samples before (blue lines, 305 K) and after (red lines, 375 K) insulator-to-metal phase transition, for a fixed antenna length $L = 150 \mu\text{m}$. For the unpatterned sample, the peak transmission at metallic phase is about 30% that of the insulator phase and the single-cycle nature of the terahertz pulse remains largely intact, indicating no resonance of the material system before and after phase transition (Figure 2a, top). For the micropatterned sample, the transmitted signal at the insulator phase is quasi-periodic, reflecting a well-defined resonance in the spectral domain. Raising the temperature all the way to the metallic still does not turn off transmission completely, leaving about 30% of amplitude at the peak (Figure 2a, middle). The nanopatterned sample again displays a quasi-periodic waveform when the film is in the insulating phase, with its amplitude similar to that of the micropatterned sample. Strikingly, for the nanopatterned sample, the transmission is turned off completely when phase turns metallic (Figure 2a, bottom).

Comparing Fourier-transformed transmission spectra for the $w = 27 \mu\text{m}$ sample (Figure 2b) and 450 nm width sample (Figure 2c) helps identify, at least qualitatively, why the nanopatterned case gives rise to so much extinction with increasing temperature and phase transition. Initially, at lower temperature, both micro- and nanopatterned samples retain resonant spectral characteristics albeit showing small

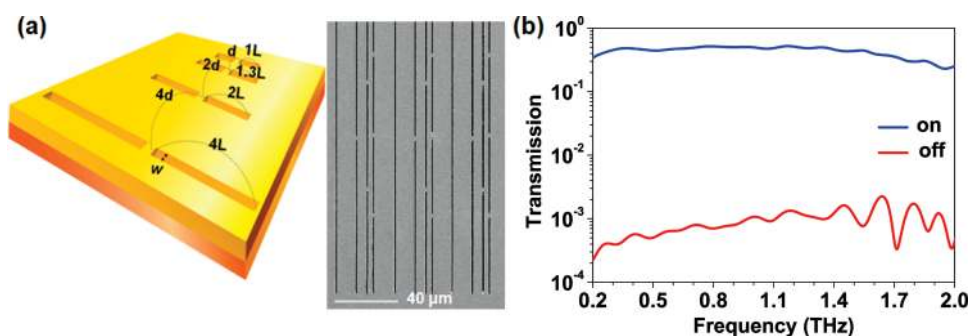


FIGURE 3. Ultra-broad-band active metamaterial at terahertz frequencies. (a) Schematics for broad-band gold resonator patterns on a VO_2 thin film (left). Scanning electron microscopy (SEM) image of a nanoresonator pattern sample (350 nm width and 50, 65, 100, and 200 μm lengths with 3, 7, 13 μm separations, respectively). (b) The logarithmic plot for transmittances of the ultra-broad-band resonator on VO_2 film at the frequency of 0.2–2.0 THz for 305 K (blue lines) and 375 K (red lines).

shifts toward lower frequencies with increasing temperature. At higher temperature, the micropatterned sample still maintains a resonant character and the transmitted intensity saturates at about 10% that of the initial one. The micropatterned sample is in addition affected by the sapphire substrate below the metallic phase, forming an averaged, albeit weak, resonance. In stark contrast, the nanopatterned sample allows the extinction to fall by another 2 orders of magnitudes, almost to the noise level over the whole spectral band. This colossal extinction results from the drastic change in the dielectric environment, which disables resonant electromagnetic wave funneling through the antenna at the observed frequency range. The shutting-off of the antenna can be visualized when we examine the enhanced current flowing beneath the resonator, as the substrate turns metallic (see Supporting Information for further detail).

We now discuss hysteresis curves at the resonant frequency formed by a complete heating and cooling circle, for bare, micropatterned, and nanopatterned samples. Since an ideal hysteresis curve with huge modulation ratio at a sharply defined critical input can form the basis of bistable switching systems,⁴⁴ identifying possible advantages of nanopatterning regarding hysteresis has technological implications. Displayed in Figure 2d are hysteresis curves for transmission at 0.4 THz for bare, $w = 27 \mu\text{m}$, $w = 1 \mu\text{m}$, and $w = 450 \text{ nm}$ patterned samples, respectively, as a function of temperature. Both bare and micropatterned samples display hysteresis curves with only one-order of transmission decrease. Striking changes in the hysteresis curves are seen for the 1 μm and 450 nm width cases, not only in terms of the enhanced dynamic range discussed earlier but also in terms of the apparent shift of the hysteresis curve toward lower temperature. This shift does not reflect the intrinsic property change of VO_2 . Rather, it is caused by the nanopatterned sample being more sensitive to smaller changes in the dielectric constant of VO_2 compared with bulk sample, because of the lack of the thin film interference effect.

Having demonstrated that the nanoantenna array with a *single antenna per unit cell* enables orders of magnitudes larger extinction as a function of temperature, we proceed

to investigate the case of multiantennas per unit cell, constructed with coupled antennas of different lengths (Figure 3a), inspired by log-periodic antennas.⁴⁵ Our design for broad band performance is expected to maximize the spectral width while still retaining excellent extinction ratio.⁴⁶ Each unit cell of 40 μm width is composed of ten 350 nm width nano slot antennas with four different lengths from 50 to 200 μm (Figure 3a). It should be stressed that having such a large number of antennas per unit cell, still with a very small coverage of only 3.5%, is possible because we pattern with nanoscale widths.

The transmission spectrum for insulating VO_2 indeed shows an ultra-broad-band spectrum of over 1 decade covering between 0.2 and 2 THz, meeting our expectation (Figure 3b, blue line). When the underlying film is in the metallic state, transmission is successfully suppressed over the whole spectrum (Figure 3b), with the extinction ratio reaching up to 1000 to 1. In analogy with log periodic antennas, the strong interantenna interaction facilitated by close-packing within the supercell is responsible for this ultra-broad-band performance. Furthermore, the subwavelength supercell period of choice, 40 μm , pushes the Rayleigh minima out of our spectral range of 0.2–2 THz.

In conclusion, we demonstrate metamaterials having ultrabroad frequency response of over 1 decade, with orders of magnitudes increased control dynamic range of 1000, up to 10000. This new class of nano-resonator-based metamaterial transforms itself from virtually transparent to completely opaque with increasing temperature, achieving functionalities totally different from the simple response sum of metal and VO_2 thin film against the stimulus, eliminating the multiple interference problem that has plagued thin film application to long wavelength regime. Two of the most important demands for present metamaterials research, that is, ultra-broad-band operation and full transmission/extinction control, are successfully met in our terahertz nanoresonator metamaterial. Our structure enables nanoscale thin film technology to fully enter into long wavelength domain, and we foresee a wide range of applications in areas where

perfect modulation, giant nonlinearity, switching, filtering, and active intelligent Fourier engineering in broad far-IR bands are desired.

Acknowledgment. We acknowledge helpful discussions with Dr. Y. D. Suh, Professor S. Hohng, and Dr. S. W. Nam. This work was supported by the Korea Science and Engineering Foundation (KOSEF) (SRC, No. R11-2008-095-01000-0) and the Korea Research Foundation (KRF) grant funded by the Korea government (MEST) (No. 2009-0071309), KICOS (GRL, K20815000003), Seoul Science Fellowship and the Seoul R&BD Program (10543). The authors gratefully acknowledge the SEMITEC, Innchips Technology and Tnест in offering excellent thermistors.

Supporting Information Available. Electric field distribution by finite difference time domain simulations. This material is available free of charge via the Internet at <http://pubs.acs.org>.

REFERENCES AND NOTES

- Xiong, Y.; Liu, Z.; Sun, C.; Zhang, X. Two-Dimensional Imaging by Far-Field Superlens at Visible Wavelengths. *Nano Lett.* **2007**, *7* (11), 3360–3365.
- Liu, N.; Weiss, T.; Mesch, M.; Langguth, L.; Eigenthaler, U.; Hirscher, M.; Soñnichsen, C.; Giessen, H. Planar Metamaterial Analogue of Electromagnetically Induced Transparency for Plasmonic Sensing. *Nano Lett.* **2010**, *10*, 1103–1107.
- Kim, D.-S.; Heo, J.; Ahn, S.-H.; Han, S. W.; Yun, W. S.; Kim, Z. H. Real-Space Mapping of the Strongly Coupled Plasmons of Nanoparticle Dimers. *Nano Lett.* **2009**, *9* (10), 3619–3625.
- Sundaramurthy, A.; Schuck, P. J.; Conley, N. R.; Fromm, D. P.; Kino, G. S.; Moerner, W. E. Toward Nanometer-Scale Optical Photolithography: Utilizing the Near-Field of Bowtie Optical Nanoantennas. *Nano Lett.* **2006**, *6* (3), 355–360.
- Smith, D. R.; Pendry, J. B.; Wiltshire, M. C. K. Metamaterials and negative refractive index. *Science* **2004**, *305* (5685), 788–792.
- Schwanecke, A. S.; Fedotov, V. A.; Khardikov, V. V.; Prosvirnin, S. L.; Chen, Y.; Zheludev, N. I. Nanostructured Metal Film with Asymmetric Optical Transmission. *Nano Lett.* **2008**, *8* (9), 2940–2943.
- Driscoll, T.; Kim, H.-T.; Chae, B.-G.; Kim, B.-J.; Lee, Y.-W.; Jokerst, N. M.; Palit, S.; Smith, D. R.; Di Ventra, M.; Basov, D. N. Memory Metamaterials. *Science* **2009**, *325* (5947), 1518–1521.
- Chen, H.-T.; Padilla, W. J.; Zide, J. M. O.; Gossard, A. C.; Taylor, A. J.; Averitt, R. D. Active terahertz metamaterial devices. *Nature* **2006**, *444* (7119), 597–600.
- MacDonald, K. F.; Samson, Z. L.; Stockman, M. I.; Zheludev, N. I. Ultrafast active plasmonics. *Nat. Photonics* **2009**, *3* (1), 55–58.
- Gansel, J. K.; Thiel, M.; Rill, M. S.; Decker, M.; Bade, K.; Saile, V.; von Freymann, G.; Linden, S.; Wegener, M. Gold Helix Photonic Metamaterial as Broadband Circular Polarizer. *Science* **2009**, *325* (5947), 1513–1515.
- Han, J.; Gu, J.; Lu, X.; He, M.; Xing, Q.; Zhang, W. Broadband resonant terahertz transmission in a composite metal-dielectric structure. *Opt. Express* **2009**, *17* (19), 16527–16534.
- Kim, H. T.; Chae, B. G.; Youn, D. H.; Maeng, S. L.; Kim, G.; Kang, K. Y.; Lim, Y. S. Mechanism and observation of Mott transition in VO₂-based two- and three-terminal devices. *New J. Phys.* **2004**, *6* (5), 52.
- Kim, B. J.; Lee, Y. W.; Choi, S.; Chae, B. G.; Kim, H. T. Analysis of the surface morphology and the resistance of VO₂ thin films on M-plane Al₂O₃. *J. Korean Phys. Soc.* **2007**, *50* (3), 653–656.
- Rini, M.; Hao, Z.; Schoenlein, R. W.; Giannetti, C.; Parmigiani, F.; Fourmaux, S.; Kieffer, J. C.; Fujimori, A.; Onoda, M.; Wall, S.; Cavalleri, A. Optical switching in VO₂ films by below-gap excitation. *Appl. Phys. Lett.* **2008**, *92* (18), 181904.
- Kubler, C.; Ehrke, H.; Huber, R.; Lopez, R.; Halabica, A.; Haglund, R. F., Jr.; Leitenstorfer, A. Coherent structural dynamics and electronic correlations during an ultrafast insulator-to-metal phase transition in VO₂. *Phys. Rev. Lett.* **2007**, *99* (11), 116401.
- Baik, J. M.; Kim, M. H.; Larson, C.; Yavuz, C. T.; Stucky, G. D.; Wodtke, A. M.; Moskovits, M. Pd-Sensitized Single Vanadium Oxide Nanowires: Highly Responsive Hydrogen Sensing Based on the Metal-Insulator Transition. *Nano Lett.* **2009**, *9* (12), 3980–3984.
- Driscoll, T.; Palit, S.; Qazilbash, M. M.; Brehm, M.; Keilmann, F.; Byung-Gyu, C.; Sun-Jin, Y.; Hyun-Tak, K.; Cho, S. Y.; Jokerst, N. M.; Smith, D. R.; Basov, D. N. Dynamic tuning of an infrared hybrid-metamaterial resonance using vanadium dioxide. *Appl. Phys. Lett.* **2008**, *93* (2), 024101.
- Dicken, M. J.; Aydin, K.; Pryce, I. M.; Sweatlock, L. A.; Boyd, E. M.; Walavalkar, S.; Ma, J.; Atwater, H. A. Frequency tunable near-infrared metamaterials based on VO₂ phase transition. *Opt. Express* **2009**, *17* (20), 18330–18339.
- Kroemer, H. A proposed class of hetero-junction injection lasers. *Proc. IEEE* **1963**, *51* (12), 1782–1783.
- Kang, W. N.; Kim, H.-J.; Choi, E.-M.; Jung, C. U.; Lee, S.-I. MgB₂ Superconducting Thin Films with a Transition Temperature of 39 K. *Science* **2001**, *292* (5521), 1521–1523.
- Morin, F. J. Oxides which show a metal-to-insulator transition at the neel temperature. *Phys. Rev. Lett.* **1959**, *3* (1), 34–36.
- Debye, G.; de Gennes, P.-G.; Brochard-Wyart, F. The Life and Death of “Bare” Viscous Bubbles. *Science* **1998**, *279* (5357), 1704–1707.
- van der Molen, S. J.; Liao, J.; Kudernac, T.; Agustsson, J. S.; Bernard, L.; Calame, M.; van Wees, B. J.; Feringa, B. L.; Schoonenberger, C. Light-Controlled Conductance Switching of Ordered Metal-Molecule-Metal Devices. *Nano Lett.* **2008**, *8* (1), 76–80.
- Dani, K. M.; Ku, Z.; Upadhyay, P. C.; Prasadkumar, R. P.; Brueck, S. R. J.; Taylor, A. J. Subpicosecond Optical Switching with a Negative Index Metamaterial. *Nano Lett.* **2009**, *9* (10), 3565–3569.
- Kleine-Ostmann, T.; Dawson, P.; Pierz, K.; Hein, G.; Koch, M. Room-temperature operation of an electrically driven terahertz modulator. *Appl. Phys. Lett.* **2004**, *84* (18), 3555–3557.
- Parkinson, P.; Joyce, H. J.; Gao, Q.; Tan, H. H.; Zhang, X.; Zou, J.; Jagadish, C.; Herz, L. M.; Johnston, M. B. Carrier Lifetime and Mobility Enhancement in Nearly Defect-Free Core-Shell Nanowires Measured Using Time-Resolved Terahertz Spectroscopy. *Nano Lett.* **2009**, *9* (9), 3349–3353.
- Rusina, A.; Durach, M.; Nelson, K. A.; Stockman, M. I. Nanoconcentration of terahertz radiation in plasmonic waveguides. *Opt. Express* **2008**, *16* (23), 18576–18589.
- Lee, J. W.; Seo, M. A.; Sohn, J. Y.; Ahn, Y. H.; Kim, D. S.; Jeoung, S. C.; Lienau, C.; Park, Q. H. Invisible plasmonic meta-materials through impedance matching to vacuum. *Opt. Express* **2005**, *13* (26), 10681–10702.
- Huber, A. J.; Keilmann, F.; Wittborn, J.; Aizpurua, J.; Hillenbrand, R. Terahertz near-field nanoscopy of mobile carriers in single semiconductor nanodevices. *Nano Lett.* **2008**, *8* (11), 3766–3770.
- Ren, L.; Pint, C. L.; Booshehri, L. G.; Rice, W. D.; Wang, X.; Hilton, D. J.; Takeya, K.; Kawayama, I.; Tonouchi, M.; Hauge, R. H.; Kono, J. Carbon Nanotube Terahertz Polarizer. *Nano Lett.* **2009**, *9* (7), 2610–2613.
- George, P. A.; Strait, J.; Dawlaty, J.; Shivaraman, S.; Chandrashekar, M.; Rana, F.; Spencer, M. G. Ultrafast Optical-Pump Terahertz-Probe Spectroscopy of the Carrier Relaxation and Recombination Dynamics in Epitaxial Graphene. *Nano Lett.* **2008**, *8* (12), 4248–4251.
- Hu, Y.; Xiang, J.; Liang, G.; Yan, H.; Lieber, C. M. Sub-100 Nanometer Channel Length Ge/Si Nanowire Transistors with Potential for 2 THz Switching Speed. *Nano Lett.* **2008**, *8* (3), 925–930.
- Seo, M. A.; Park, H. R.; Koo, S. M.; Park, D. J.; Kang, J. H.; Suwal, O. K.; Choi, S. S.; Planken, P. C. M.; Park, G. S.; Park, N. K.; Park, Q. H.; Kim, D. S. Terahertz field enhancement by a metallic nano slit operating beyond the skin-depth limit. *Nat. Photonics* **2009**, *3* (3), 152–156.
- Gunter, G.; Anappara, A. A.; Hees, J.; Sell, A.; Biasiol, G.; Sorba, L.; De Liberato, S.; Ciuti, C.; Tredicucci, A.; Leitenstorfer, A.

- Huber, R. Sub-cycle switch-on of ultrastrong light-matter interaction. *Nature* **2009**, *458* (7235), 178–181.
- (35) Born, M.; Wolf, E., *Principles of Optics*. 1964: Press, Oxford.
- (36) Garcia-Vidal, F. J.; Moreno, E.; Porto, J. A.; Martin-Moreno, L. Transmission of light through a single rectangular hole. *Phys. Rev. Lett.* **2005**, *95* (10), 103901.
- (37) Lee, J. W.; Seo, M. A.; Park, D. J.; Kim, D. S.; Jeoung, S. C.; Lienau, C.; Park, Q. H.; Planken, P. C. M. Shape resonance omnidirectional terahertz filters with near-unity transmittance. *Opt. Express* **2006**, *14* (3), 253–1259.
- (38) Lee, J. W.; Seo, M. A.; Kang, D. H.; Khim, K. S.; Jeoung, S. C.; Kim, D. S. Terahertz electromagnetic wave transmission through random arrays of single rectangular holes and slits in thin metallic sheets. *Phys. Rev. Lett.* **2007**, *99* (13).
- (39) Seo, M. A.; Adam, A. J. L.; Kang, J. H.; Lee, J. W.; Ahn, K. J.; Park, Q. H.; Planken, P. C. M.; Kim, D. S. Near field imaging of terahertz focusing onto rectangular apertures. *Opt. Express* **2008**, *16* (25), 20484–20489.
- (40) Liu, H.; Lalanne, P. Microscopic theory of the extraordinary optical transmission. *Nature* **2008**, *452* (7188), 728–731.
- (41) Exter, M. V.; Fattinger, C.; Grischkowsky, D. Terahertz time-domain spectroscopy of water vapor. *Opt. Lett.* **1989**, *14* (20), 1128–1130.
- (42) Han, P. Y.; Zhang, X. C. Free-space coherent broadband terahertz time-domain spectroscopy. *Meas. Sci. Technol.* **2001**, *12* (11), 1747–1756.
- (43) Hendry, E.; Koeberg, M.; O'Regan, B.; Bonn, M. Local Field Effects on Electron Transport in Nanostructured TiO₂ Revealed by Terahertz Spectroscopy. *Nano Lett.* **2006**, *6* (4), 755–759.
- (44) Gibbs, H. M. *Optical bistability: controlling light with light*; Academic Press, Inc.: Orlando, FL, 1985.
- (45) Balanis, C. A. *Antenna theory: analysis and design*; Wiley: New York, 1997.
- (46) Park, H. R.; Park, Y. M.; Kim, H. S.; Kyoung, J. S.; Seo, M. A.; Park, D. J.; Ahn, Y. H.; Ahn, K. J.; Kim, D. S. Terahertz Nano-Resonators: Giant Field Enhancement and Ultrabroadband Performance. *Appl. Phys. Lett.* **2010**, *96*, 121106.